

Domain growth in partially melted bulk

$\text{Nd}_{1+x}\text{Ba}_{2-x}\text{Cu}_3\text{O}_{7-\delta}$

M. MARELLA, M. TOMASELLI, F. GEROLIN, B. MOLINAS,
B. BURDET FABRIS, L. MEREGALLI

Enirisorse-Centro Ricerche Venezia, via delle industrie 39, P.to Marghera, Venice, Italy

Domain growth of bulk partially melted $\text{Nd}_{1+x}\text{Ba}_{2-x}\text{Cu}_3\text{O}_{7-\delta}$ in air was found to be severely limited by liquid-phase segregation and losses. The use of a reduced oxygen pressure greatly improved the stoichiometry control, leading to the formation of well-developed domains and enhanced superconducting properties. Direct nucleation of $\text{Nd}_{1+x}\text{Ba}_{2-x}\text{Cu}_3\text{O}_{7-\delta}$ from the liquid phase by dissolution of $\text{Nd}_2\text{BaCuO}_5$ and a spiral growth mechanism in three perpendicular directions of the platelets stacked in the domains, are suggested.

1. Introduction

Partial melting processing is the most prominent technique for obtaining bulk high- T_c superconductors with the correct texture required for large current transportation.

A thermal procedure without an imposed temperature gradient enabled $\text{YBa}_2\text{Cu}_3\text{O}_{7-\delta}$ bars to be obtained with a domain structure extended in the centimetre size range [1]. Within a single domain, $\text{YBa}_2\text{Cu}_3\text{O}_{7-\delta}$ platelets are parallel to each other and stacked along the c -axis. The J_c at 4.2 K and $H = 1$ T is $2 \times 10^5 \text{ A cm}^{-2}$. Different domains meet at high-angle boundaries, thus severely reducing the current transport capability.

Morita *et al.* [2] proposed single-crystal or melt-textured $\text{SmBa}_2\text{Cu}_3\text{O}_{7-\delta}$ or $\text{NdBa}_2\text{Cu}_3\text{O}_{7-\delta}$ as an effective seed for $\text{YBa}_2\text{Cu}_3\text{O}_{7-\delta}$ growth as a consequence of the higher peritectic decomposition temperature and the similarity of lattice parameters. More recently, Yoo *et al.* [3] studied melt–powder–melt–growth processing of $\text{NdBa}_2\text{Cu}_3\text{O}_{7-\delta}$ in 1% O_2 in argon, obtaining $J_c = 2 \times 10^4 \text{ A cm}^{-2}$ at 77 K and 2 T with H parallel to the c -axis. With a higher J_c than $\text{YBa}_2\text{Cu}_3\text{O}_{7-\delta}$ up to 4 T, this material is a strong candidate to overcome the present limitation of melt-processed bulk $\text{YBa}_2\text{Cu}_3\text{O}_{7-\delta}$ for current transport and permanent magnets applications.

The purpose of the present work is to analyse the microstructural properties of $\text{Nd}_{1+x}\text{Ba}_{2-x}\text{Cu}_3\text{O}_{7-\delta}$ as a function of partial melting procedures and to derive possible similarities with the spiral growth mechanism found for $\text{YBa}_2\text{Cu}_3\text{O}_{7-\delta}$ [4].

2. Experimental procedure

$\text{Nd}_{1+x}\text{Ba}_{2-x}\text{Cu}_3\text{O}_{7-\delta}$ powder was prepared by conventional solid-state sintering of a stoichiometric mix-

ture of $\text{Nd}(\text{NO}_3)_3 \cdot 6 \text{ H}_2\text{O}$ (Strem Chemicals, 99.9%), BaCO_3 and CuO (Johnson Matthey, Grade 1, 99.999%). The powders were dry mixed in an agate mortar and calcined in an alumina boat at 1223 K for 3 h, in air flowing at $20 \text{ dm}^3 \text{ h}^{-1}$. After crushing, the powders were reheated to 1243 K for 2 h in air and cooled in flowing oxygen ($60 \text{ dm}^3 \text{ h}^{-1}$) then held at 873 K for 10 h. Several pellets of diameter 30 mm and height 6–7 mm were prepared by pressing at 300 MPa. They were fired at the maximum temperature of 1243 K with the same heating schedule of the powders. Some bars of $28 \times 3 \times 3 \text{ mm}^3$ were derived from the pellets.

The bars were put in an alumina boat and held in an inclined position by alumina supports. The supports were obtained from near full-density hot-pressed samples. Some preliminary tests (1423 K for 15 min and 1473 K for 30 min) enabled the peak temperature to be defined in order to avoid excessive liquid-phase formation and bar deformation. Afterwards, the bars were fired by a single-step partial melting procedure. They were initially very quickly fired in air (flowing at $60 \text{ dm}^3 \text{ h}^{-1}$) to 1473 K, held for some minutes (15 min), quickly cooled to 1393 K, slightly above the peritectic decomposition temperature ($1363 \pm 10 \text{ K}$ [5]), extremely slowly cooled (0.5 K h^{-1}) to 1321 K, then cooled to 1023 K at 20 K h^{-1} . Afterwards the atmosphere was changed to flowing oxygen ($60 \text{ dm}^3 \text{ min}^{-1}$), the samples were cooled to 873 K, held for 24 h and cooled to room temperature. Because excessive liquid-phase formation occurred and the shape of the resulting was severely deformed by collapse of the external surface parallel to the alumina support, the procedure was modified by lowering the peak temperature to 1433 K and prolonging the slow cooling down to 1268 K, with all the other steps unmodified.

On the basis of microstructural observations and magnetic measurements results (see later for discussion), a different procedure was adopted: the bars were fired under $p(\text{O}_2) = 1.3$ mbar (measured by a Pirani vacuum meter). The heating schedule was substantially similar, taking into account the lower peritectic decomposition temperature (see below for discussion). The major modifications concerned the broadening of the range of temperatures over which 0.5 K h^{-1} cooling occurred and the additional extensive oxygenation at 623 K.

The following characterization was performed: X-ray diffraction (XRD) patterns were taken of powders after crushing and sieving below $40 \mu\text{m}$. The patterns were obtained by a powder diffractometer equipped with a graphite crystal monochromator using a $\text{CuK}\alpha$ X-ray radiation source. Samples were run with the diffractometer in step-scan mode with a step interval of $0.02^\circ 2\theta$ and a count rate of 1 s per step over the range of 5° – $90^\circ 2\theta$. The Rietveld full-profile analysis was applied using the crystallographic data found in the literature [6].

Optical micrographs were taken of polished samples under polarized light with crossed Nicols.

Scanning electron microscopy (SEM) observations were performed on as-grown surfaces or fracture surfaces without gold sputtering. Electron probe microscope analysis (EPMA) allowed semiquantitative chemical analysis and phase determination.

Simultaneous differential thermal and thermogravimetric analysis (DTA/DTG) were performed on alumina crucibles, either on powders or small bars, under 1.3 mbar oxygen pressure with 5 K min^{-1} heating rate up to 1373 K. Kaolin was used as reference material.

Susceptibility measurements were performed by a d.c. SQUID magnetometer from 4.2–95 K with an applied magnetic field of 1 mT.

3. Results and discussion

From the literature [7] it is known that for stoichiometric 1:2:3 compositions the superconductivity disappears at the orthorhombic-to-tetragonal phase transition which occurs at $\delta = 0.45$. On the other hand [8], solid solution exists in $\text{Nd}_{1+x}\text{Ba}_{2-x}\text{Cu}_3\text{O}_{7-\delta}$ with the solubility limit of $0.04 \leq x \leq 0.6$ at 1163 K in air and that superconductivity appears up to $x \approx 0.4$ when it is oxygen annealed. From $x > 0.1$, there is a significant depression of T_c from 93 K and for $x < 0.1$ there is no substantial decrease in T_c within experimental error.

The X-ray pattern of our precursor powders is reported in Fig. 1. Using Takita *et al.*'s assumption of oxygen content in $\text{NaBa}_2\text{Cu}_3\text{O}_7$ [6], the lattice parameters determined by Rietveld analysis were $a = 0.39095 \text{ nm}$, $b = 0.38644 \text{ nm}$ and $c = 1.17308 \text{ nm}$. The comparison with Takita *et al.*'s data shows a stoichiometry near $\text{Nd}_{1.1}\text{Ba}_{1.9}\text{Cu}_3\text{O}_7$, with orthorhombic symmetry.

Proper stoichiometry control thus appears to be a major problem in partial melting processing of $\text{Nd}_{1+x}\text{Ba}_{2-x}\text{Cu}_3\text{O}_{7-\delta}$ with respect to $\text{YBa}_2\text{Cu}_3\text{O}_{7-\delta}$. We briefly recall that this technique consists in keeping the sample for a short time above the peritectic decomposition temperature, where a liquid phase and an insulating 2–1–1 phase are formed, and in allowing the recombination and domain growth of the superconducting phase by slow cooling through the peritectic point.

Because the peritectic decomposition temperature of $\text{Nd}_{1+x}\text{Ba}_{2-x}\text{Cu}_3\text{O}_{7-\delta}$ in air occurs 72 K higher than $\text{YBa}_2\text{Cu}_3\text{O}_{7-\delta}$, liquid-phase segregation due to the lower viscosity, and chemical reactivity towards the supports due to higher diffusion coefficients, can readily occur and actually were experimentally verified.

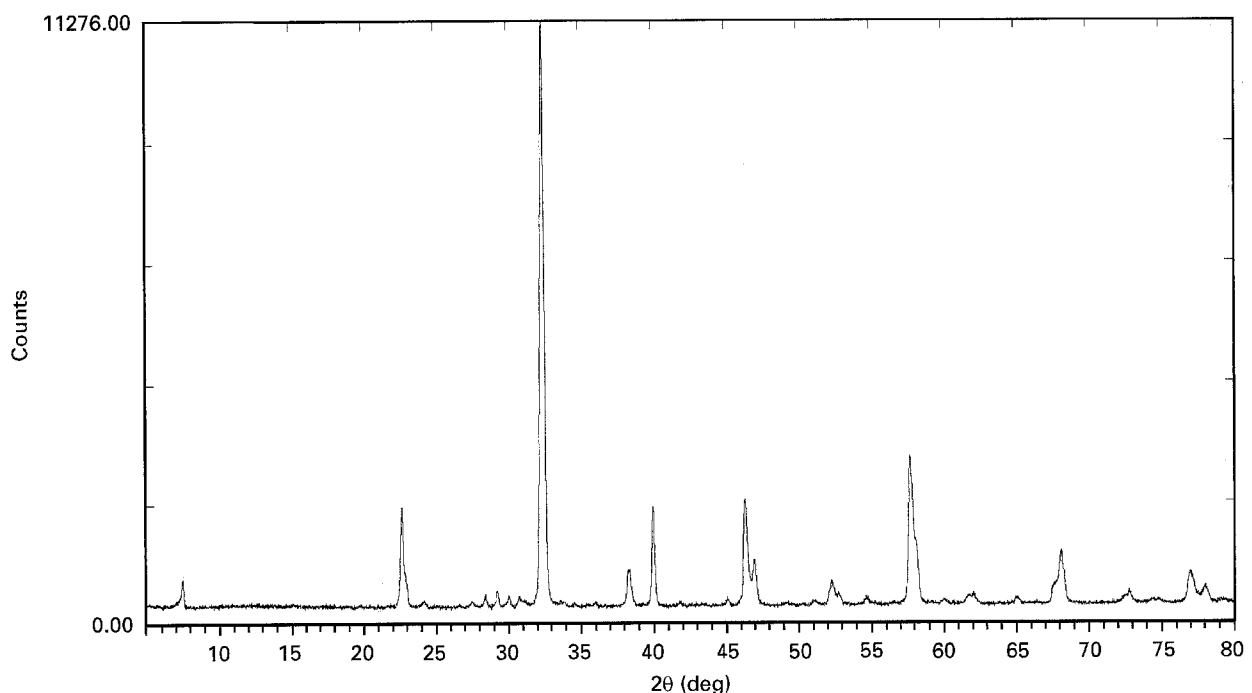


Figure 1 XRD pattern of $\text{Nd}_{1+x}\text{Ba}_{2-x}\text{Cu}_3\text{O}_{7-\delta}$ powders.

Moreover, while $\text{YBa}_2\text{Cu}_3\text{O}_{7-\delta}$ is a point composition, $\text{Nd}_{1+x}\text{Ba}_{2-x}\text{Cu}_3\text{O}_{7-\delta}$ is a solid solution. During the domain growth following the model suggested elsewhere [4], local inhomogeneities in the liquid phase can only alter the growth rates of platelets in different directions. If the same growth mechanism was operative (see later for discussion), this could lead to structures modulated in composition, which may adversely affect the superconducting properties.

After the thermal treatments in air, the samples show almost invariably characteristic deformations. On the whole the bars retain their parallelepiped shape, but the surface parallel to the one in contact with the alumina support sinks generally along the medium directrix, leaving, on a microscopic level, a needle-like structure, as shown in Fig. 2. Other interesting features are reported in Figs 2 and 3. In general, in all the micrographs, a situation of incomplete peritectic recomposition, according to Reaction 1, is verified

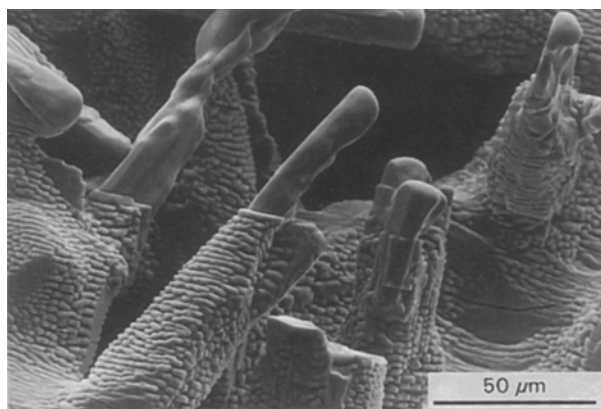
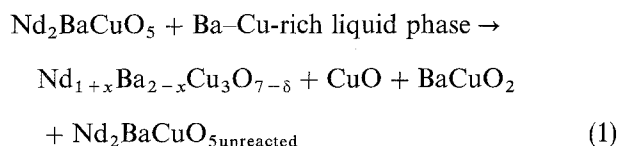


Figure 2 Scanning electron micrograph of the upper surface of a bar processed in air. The interrupted growth of a domain with needle-like $\text{Nd}_2\text{BaCuO}_5$ inclusions is shown.

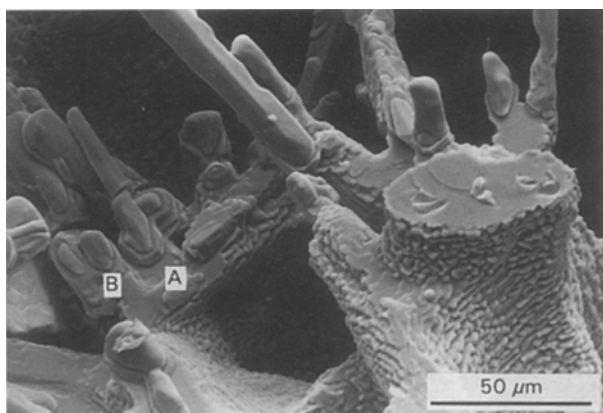


Figure 3 The same surface as in Fig. 2. (a) Octagonal-shaped macrospiral growing around a $\text{Nd}_2\text{BaCuO}_5$ inclusion. (b) Octagonal-shaped macrospiral distorted during growth by two $\text{Nd}_2\text{BaCuO}_5$ inclusions.

As a consequence of the higher temperatures and in association with the long-term treatment, the Ba-Cu-rich liquid phase is depleted from the surface and impregnates the alumina support. Fig. 4 shows a prismatic crystal of $\text{Nd}_2\text{BaCuO}_5$, identified by EPMA, with the liquid phase washed away. On the base of the crystal the liquid phase reacted with it, forming $\text{Nd}_{1+x}\text{Ba}_{2-x}\text{Cu}_3\text{O}_{7-\delta}$, and surrounded it giving the beginning of a domain structure. The domain structure is stacking of platelets of superconducting phase. For bulk $\text{YBa}_2\text{Cu}_3\text{O}_{7-\delta}$, the direct nucleation from the liquid phase, while Y_2BaCuO_5 dissolves in it, was suggested [9]. Moreover, a model of growth of the domains was proposed [4], in which a pre-existing platelet growing with a spiral growth mechanism provides information about the c -axis direction to the nucleus of a second platelet, and this situation can be extended to the n number of platelets in the domain. Evidence of spiral growth in two perpendicular directions was provided, and a subsequent work on sol-gel $\text{YBa}_2\text{Cu}_3\text{O}_{7-\delta}$ microspheres [10] provided evidence of spiral growth in three perpendicular directions, as an extension of the above model. Furthermore, the morphology of the as-grown (001) surface could be explained on the basis of the periodic bond chain (PBC) theory [11, 12] with the transition from a rough to a smooth interface playing a fundamental role and the step heights in the submicrometre size range were explained by the Khulmann-Wilsdorf giant screw dislocations mechanism, caused by an impurity-induced lattice-constant gradient [13]. A summary of spiral characteristics in partially melted bulk $\text{YBa}_2\text{Cu}_3\text{O}_{7-\delta}$, together with a comparison with spirals in single crystals, thin and thick films, was also given [4].

It seems reasonable to keep the above model as a hypothesis of work, considering the similarities of the two materials. Fig. 5 shows a domain whose growth was interrupted by the lack of liquid phases. The hole in the bottom right corner suggests this situation. The lamellar structure is given by a - b planes growing at a rate higher than the growth along the c -axis. The lack of liquid in the neighbourhood of the surface of the sample forbids the coarsening of the platelets along the c -axis, so that the thickness of the outermost platelets is 1.5–2 μm . The interrupted growth of the domains is also clearly shown in Figs 2

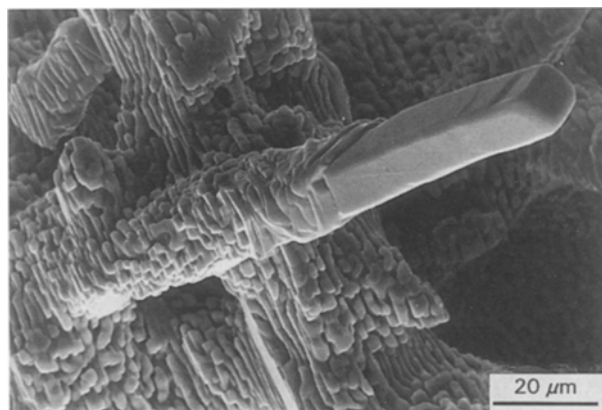


Figure 4 Prismatic crystal of $\text{Nd}_2\text{BaCuO}_5$ unreacted owing to the lack of liquid phase.

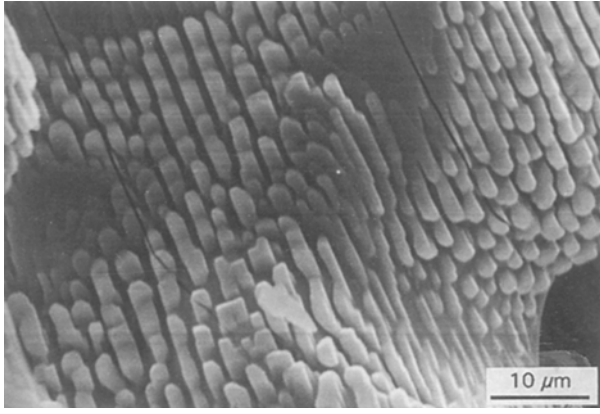


Figure 5 Stacking of platelets in a domain on the bar surface. Platelet coarsening is prevented by the lack of liquid.

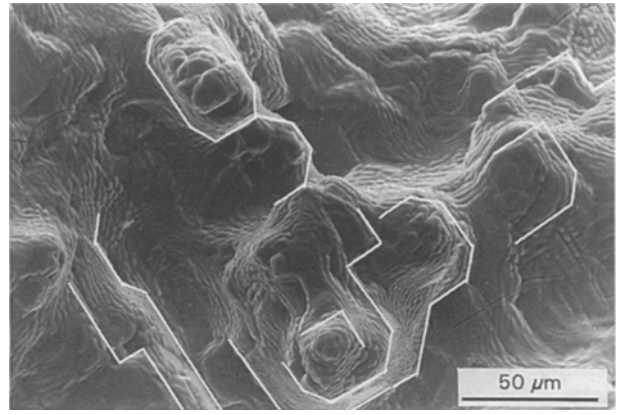


Figure 7 As-grown upper surface of a bar processed in air; denser zone. White lines underline the intrinsic order in the growth. Longer perpendicular lines are drawn on the strongest PBC directions. Shorter 45° inclined lines refer to the next strongest PBC directions.

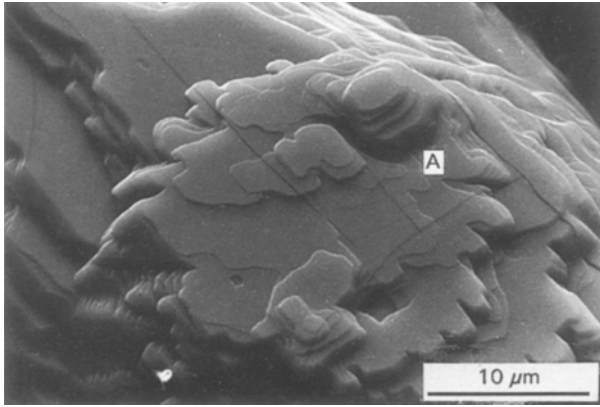


Figure 6 Macrospiral transition from octagonal to rectangular, A.

and 3. In particular, the latter figure shows other interesting features, related to the incomplete dissolution of $\text{Nd}_2\text{BaCuO}_5$ phase. A macrospiral growing with octagonal shape around an $\text{Nd}_2\text{BaCuO}_5$ inclusion is marked by "A". In its proximity, another octagonal-shaped macrospiral was distorted during the growth by two $\text{Nd}_2\text{BaCuO}_5$ inclusions ("B"). According to the PBC theory, on decreasing the roughness there is a transition from circular to octagonal to square (or rectangular) in the morphology of the spirals. Fig. 6 shows the transition from octagonal to rectangular on the top of the structure of the growth marked "A". When this happens, the steps follow the strongest $\langle 010 \rangle / \langle 100 \rangle$ PBC directions where the kink density is lower. According to the Jackson factor [14]

$$\alpha = \xi L / k T_0 \quad (2)$$

where ξ is related to the crystallographic anisotropy, L is the latent heat of melting, k is the Boltzmann constant and T_0 the equilibrium temperature, this transition is associated with a decrease in the temperature of growth.

Figs 2, 3 and 4 demonstrate that the growth of the platelets proceeds independently of the crystallographic orientation of $\text{Nd}_2\text{BaCuO}_5$ crystals, even though they participate in the growth of the platelets through their own dissolution. All the platelets with

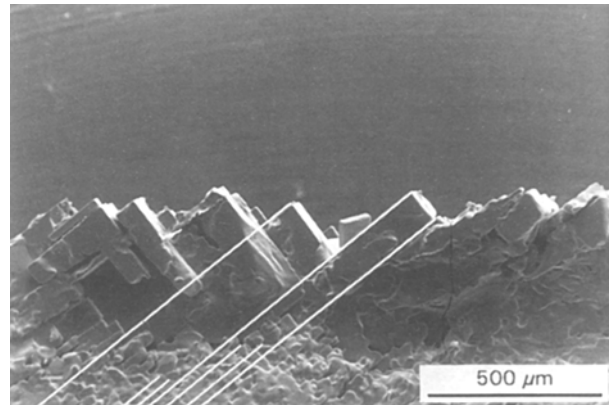


Figure 8 Aluminium-doped pseudo single crystals inducing the growth of a domain (bottom). White lines suggest the relative orientation between the crystals and the platelets stacked in the domain.

their a - b planes are parallel in spite of a morphology full of pores and $\text{Nd}_2\text{BaCuO}_5$ inclusions.

On the same surface, in areas where, for some reason, excessive liquid loss did not happen, a denser structure could be observed, Fig. 7. This structure is similar to those found in $\text{YBa}_2\text{Cu}_3\text{O}_{7-\delta}$ growth [1] and, though heavily disturbed in this case, it shows a regular pattern of growth with groups of macrospirals interfering with each other and merging together. The white lines indicate a network of two perpendicular strongest PBC directions (longer segments) and 45°-next strongest PBC directions, followed by the spirals while solidificating from partially melted material.

On the opposite surface, in contact with the support, the presence of pseudo-single crystals was revealed, as shown in Fig. 8. In the case of $\text{YBa}_2\text{Cu}_3\text{O}_{7-\delta}$ single crystals, it is well known that aluminium can be dissolved from the crucible during growth and incorporated into the crystals [15]. In the case of partially melted $\text{YBa}_2\text{Cu}_3\text{O}_{7-\delta}$, the same phenomenon occurs and enables us to recall the Khulmann-Wilsdorf giant screw dislocations mechanism, caused by an impurity-induced lattice-constant gradient. In the present case, EPMA of the pseudo-single

crystals showed a mean atomic ratio Nd:Ba:Cu:Al = 1.12:1.68:2.41:0.79. These parallelepiped shaped crystals, with dimensions of hundreds of micrometres, induce the growth of a domain extending for 3 mm. Platelet stacking along the c -axis is related to the orientation of the pseudo single crystals, as shown in Fig. 8. The white lines indicate the traces of a - b planes. The link between the platelet growth and the presence of these crystals is also revealed by a closer detail, Fig. 9, where some platelets (A) are growing on bulk crystals (B) and tabular crystals (C). From both figures it is possible to determine a platelet thickness of 15–20 μm , very similar to that of $\text{YBa}_2\text{Cu}_3\text{O}_{7-\delta}$ platelets [4].

From another sample, obtained with the same heating schedule, a slab for magnetic measurements was

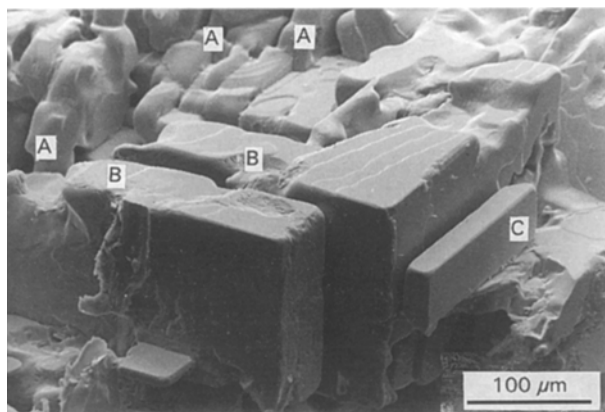


Figure 9 Closer detail of Fig. 8 showing Platelets, A, growing on bulk crystals. B, C is a tabular shaped crystal.

derived. It essentially consisted of three domains and EPMA showed a mean atomic ratio Nd:Ba:Cu = 1.27:1.85:3.06 with relevant $\text{Nd}_2\text{BaCuO}_5$ inclusions (near 50%, as determined by statistical point analysis). Susceptibility measurements are reported in Fig. 10 (curve I). With an applied field of 1 mT and $T_{c\text{ onset}} = 85$ K, the transition is very broad and the signal decreases to 4.2 K. A shielding of 55% of the total volume was estimated. This value is in fairly good agreement with EPMA measurements. From all this, the drawbacks of thermal treatment in air can be definitely assessed.

Previous work on sol-gel $\text{YBa}_2\text{Cu}_3\text{O}_{7-\delta}$ microspheres [10] showed the usefulness of using a reduced oxygen pressure in favouring a mechanism of nucleation and growth analogous to partial melting at temperatures as low as 1123–1173 K. With the purpose of defining a more convenient atmosphere, in order to lower the peritectic decomposition temperature and to limit liquid-phase losses, the same atmosphere was selected and DTA/DTG measurements in reduced oxygen pressure were made. The results are reported in Fig. 11. The peritectic decomposition temperature in $p(\text{O}_2) = 1.3$ mbar was determined as 1276 K (onset) and 1302 K (peak).

Near full-density bars were obtained by this procedure. Fig. 12 shows the fracture surface of a domain, where the stacking of the platelets along the c -axis is readily observable. The platelet thickness is between 15 and 20 μm . In Fig. 13, the polished surface of a domain is shown in polarized light with crossed Nicols. A set of perpendicular twin traces is observed. Twinning is originated by the tetragonal-to-orthorhombic transition, with $\{110\}$ as the twin plane [16]. The

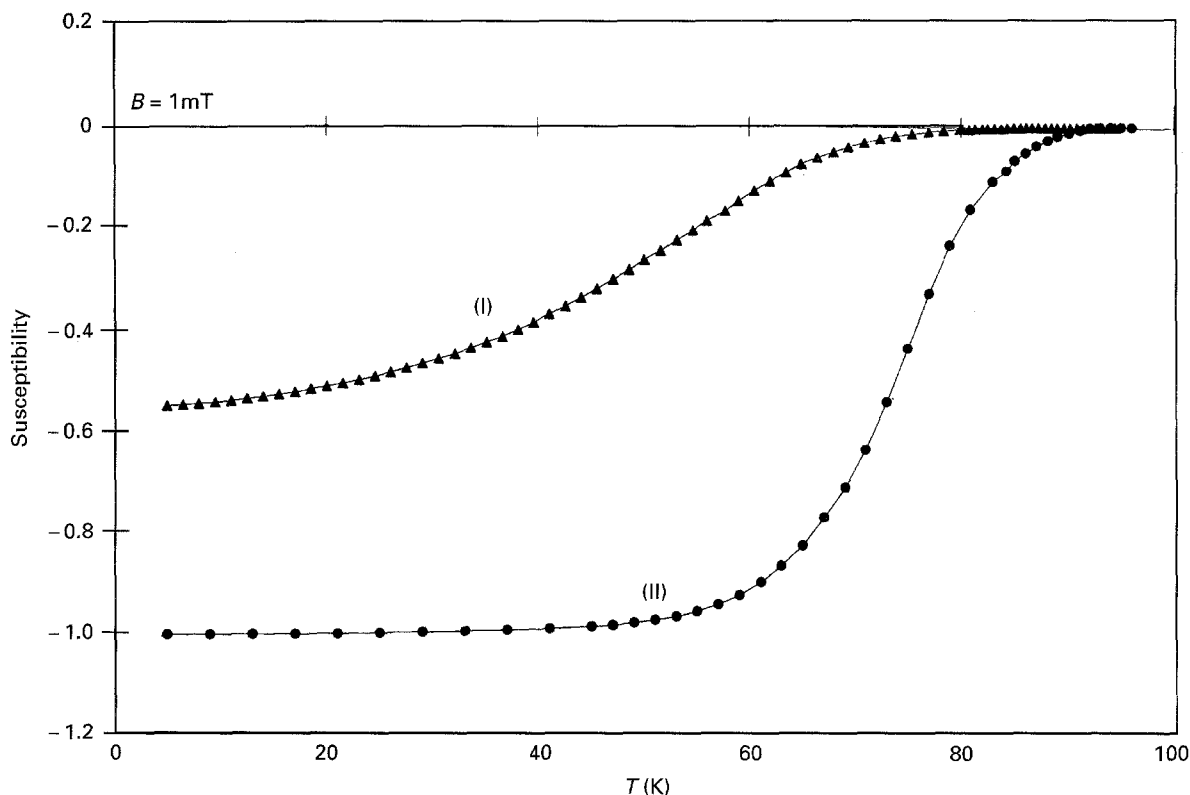


Figure 10 Zero-field cooled susceptibility versus temperature with $B = 1$ mT: (I) sample obtained by procedure in air; (II) sample obtained by procedure in reduced oxygen pressure.

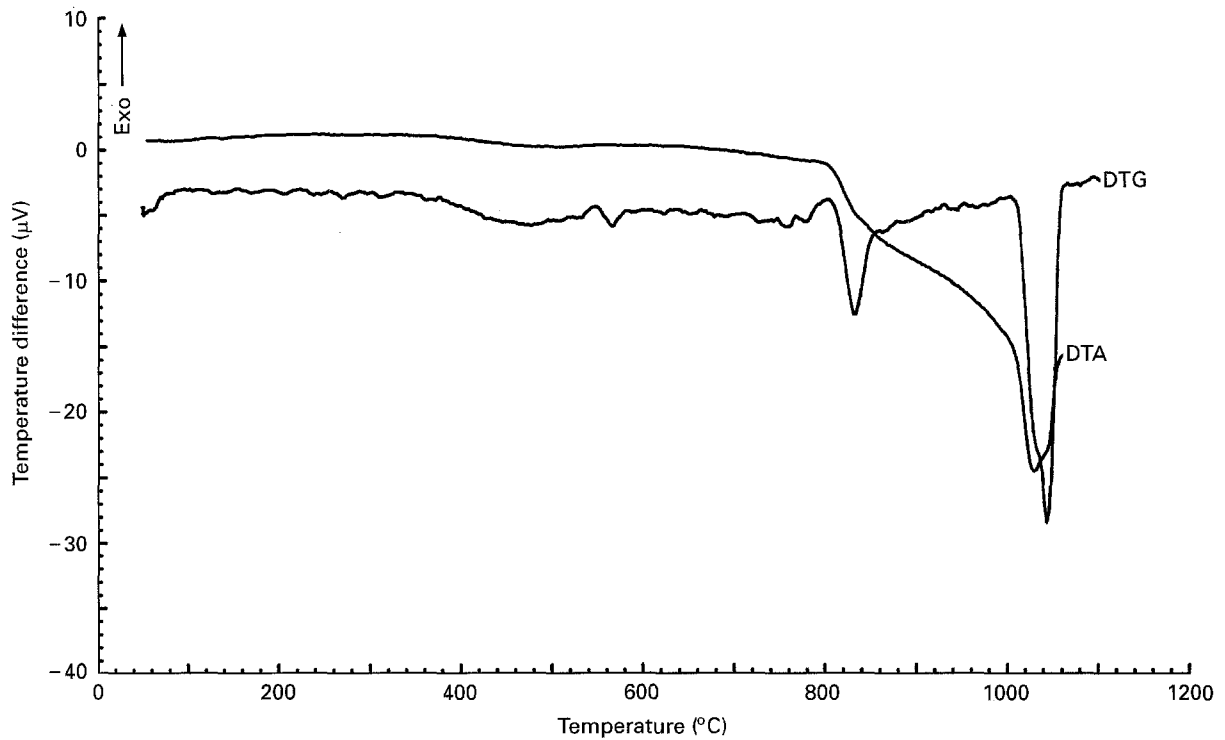


Figure 11 Simultaneous DTA/DTG analysis of $\text{Nd}_{1+x}\text{Ba}_{2-x}\text{Cu}_3\text{O}_{7-\delta}$ powders in $p(\text{O}_2) = 1.3$ mbar.

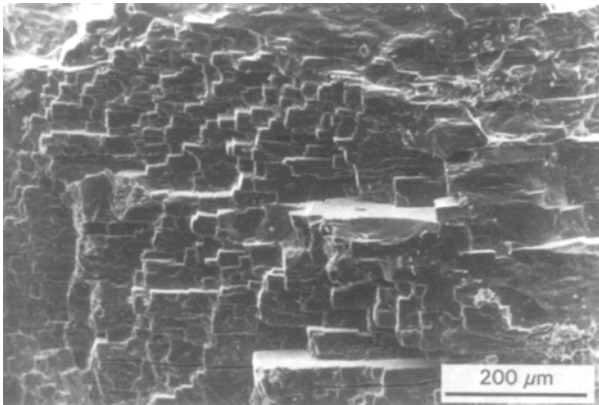


Figure 12 SEM fracture surface of a domain in a bar processed in a reduced oxygen pressure. Platelet a - b planes are distinguishable by bright grey areas.

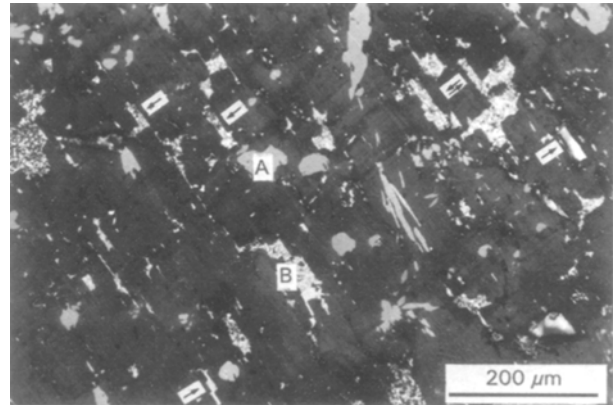


Figure 13 Optical micrograph of a domain in polarized light with crossed Nicols. A set of perpendicular twin traces is shown. A, $\text{Nd}_2\text{BaCuO}_5$ phase inclusions. B, BaCuO_2 inclusions. The arrows mark the elongation of the inclusions along twin traces.

$\{110\}$ planes give rise, on a - b planes, to a set of perpendicular lines, as observed in Fig. 13. The presence of $\text{Nd}_2\text{BaCuO}_5$ phase and interstitial Ba-Cu-rich phase is revealed. Moreover, the nucleation of secondary phases follows those directions, giving rise to crystals elongated along one or both directions, marked by arrows in the figure. The domain extension is typically of the order of $2 \times 2 \text{ mm}^2$ cross-section. The as-grown surface furnishes additional experimental evidence to the model of growth proposed for structurally similar $\text{YBa}_2\text{Cu}_3\text{O}_{7-\delta}$ compound [4]. Moreover, it is here possible to verify, in a partially melted sample, what for $\text{YBa}_2\text{Cu}_3\text{O}_{7-\delta}$ had been possible only for microspheres [10]. Fig. 14 shows a complex structure of a domain growth interrupted during growth by the lack of liquid phase. The micrograph shows one or more, probably two, platelets. With this

latter assumption, platelet thickness along the c -axis is marked in the figure by d . A structure of growth related to a spiral growth is marked "A". On the same platelet an outgrowth structure is present (O). This substructure grows by a spiral growth mechanism in three perpendicular directions. The respective ledges of growth are marked "B", "C" and "D". Spirals "A" and "B" grow along the same directions. The second platelet, marked "E", is just at the beginning of growth and appears to be misoriented with respect to a - and b -axes of the other platelet. However, the c -axis orientation is the same as in the other platelet, exactly as should occur by the proposed model [4]. In the same micrograph, some cracks due to thermal stresses, marked "F", are shown.

EPMA analysis on the domains gave a mean atomic ratio $\text{Nd}:\text{Ba}:\text{Cu} = 1.07:1.89:3.04$. The accordance

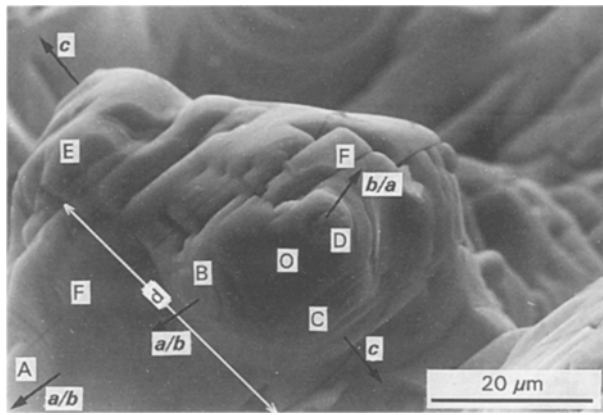


Figure 14 Platelet growth along three perpendicular directions, marked by black arrows. A, Structure of growth of the platelet with thickness, d . O, Outgrowth structure of the same platelet, with structures of growth B, C and D in perpendicular directions. F, cracks due to anisotropic thermal expansion. E, A second platelet with the same c -axis orientation, but probably misoriented along a - and b -axes.

with the stoichiometry of precursor powders, as determined by XRD, appears very good and indicative of minor liquid-phase losses. A sample of $2.2 \times 2.5 \text{ mm}^2$ cross-section and 4mm height was measured by SQUID, Fig. 10 (curve II). The $T_{c \text{ onset}}$ was 93 K and full diamagnetism was reached near 50 K. These results are in accordance with the literature [8] indicating good superconducting properties for $\text{Nd}_{1+x}\text{Ba}_{2-x}\text{Cu}_3\text{O}_{7-\delta}$ with $1 + x < 1.1$.

4. Conclusion

The advantages of the partial melting procedure for $\text{Nd}_{1+x}\text{Ba}_{2-x}\text{Cu}_3\text{O}_{7-\delta}$ in reduced oxygen pressure in comparison to a similar procedure in air were definitely assessed. The necessity of achieving a better control on the stoichiometry, in order to avoid the presence of structures modulated in composition, and to obtain a sharper superconducting transition, was also clarified. Our experiments also suggest that $\text{Nd}_{1+x}\text{Ba}_{2-x}\text{Cu}_3\text{O}_{7-\delta}$ domains grow by a spiral growth mechanism along three perpendicular directions. In this way, our previously proposed model of nucleation and growth of $\text{YBa}_2\text{Cu}_3\text{O}_{7-\delta}$ finds more experimental support. The understanding of these

phenomena represents a key factor for improving the partial melting procedures.

Acknowledgement

The authors thank Dr M. Battagliarin for Rietveld analysis on powders and Dr G. Pannocchia for DTA/DTG measurements. Professor A.S. Siri and Dr C. Ferdeghini, Department of Physics, University of Genoa, are especially thanked for magnetic measurements.

References

1. M. MARELLA, G. DINELLI, B. BURTET FABRIS and B. MOLINAS, *J. Alloys Comp.* **189** (1992) L23.
2. M. MORITA, S. TAKEBAYASHI, M. TANAKA, K. KIMURA, K. MIYAMOTO and K. SAWANO, *Adv. Supercond.* **3** (1991) 733.
3. S. I. YOO, N. SAKAI, H. TAKAICHI, T. HIGUCHI and M. MURAKAMI, *Appl. Phys. Lett.* **65** (1994) 602.
4. M. MARELLA, B. MOLINAS and B. BURTET FABRIS, *J. Mater. Sci.* **29** (1994) 3497.
5. K. OKA and H. UNOKI, *J. Crystal Growth* **99** (1990) 922.
6. K. TAKITA, H. KATOH, H. AKINAGA, M. NISHINO, T. ISHIGAKI and H. ASANO, *Jpn. J. Appl. Phys.* **27** (1988) L57.
7. H. SHAKED, B. W. VEAL, H. FABER, R. L. HITTERMAN, U. BALACHANDRAN, G. TOMLINS, H. SHI, L. MORSS and A. P. PAULINKAS, *Phys. Rev. B* **41** (1990) 4173.
8. S. I. YOO and R. W. McCALLUM, *Phys. C* **210** (1993) 157.
9. C. A. BATEMAN, L. ZHANG, H. M. CHAN and M. P. HARMER, *J. Am. Ceram. Soc.* **75** (1992) 1281.
10. M. MARELLA, B. MOLINAS, B. BURTET FABRIS, L. MEREGALLI and P. GERONTOPOULOS, *J. Mater. Sci. Lett.* **13** (1994) 1108.
11. P. HARTMAN and W. G. PERDOK, *Acta Crystallogr.* **8** (1955) 49.
12. *Idem. ibid.* **8** (1955) 521.
13. D. KUHLMANN-WILSDORF, D. PANDEY and P. KRISHNA, *Philos. Mag.* **A 00-4** (1980) 527.
14. K. A. JACKSON, "Liquid Metals and Solidification" (American Society for Metals, Cleveland, OH, 1958) p. 174.
15. T. SIEGRIST, L. F. SCHEEMEYER, J. V. WASZCZAK, N. P. SINGH, R. L. OPILA, B. BATLOGG, L. W. RUPP and D. W. MURPHY, *Phys. Rev. B* **36** (1987) 8365.
16. G. VAN TENDELOO, H. W. ZANDBERGEN, J. VAN LANDUYT and S. AMELINCKX, *Mater. Charact.* **27** (1991) 59.

Received 22 May
and accepted 1 December 1995